Solar Energy 205 (2020) 275–281

Contents lists available at ScienceDirect

Solar Energy

journal homepage: www.elsevier.com/locate/solener

# Moth-eye nanostructure PDMS films for reducing reflection and retaining flexibility in ultra-thin c-Si solar cells

Zhongliang Gao[a], Guilu Lin[b], Yongcong Chen[a], Yupeng Zheng[a], Na Sang[b], Yingfeng Li[a], Lei Chen[b], Meicheng Li[a,*]

[a] State Key Laboratory of Alternate Electrical Power System with Renewable Energy Sources, School of New Energy, North China Electric Power University, Beijing 102206, China
[b] School of Mathematics and Physics, North China Electric Power University, Beijing 102206, China

ARTICLE INFO

*Keywords:*
PDMS film
Moth-eye nanostructure
Antireflective coating
Finite element method
Flexible ultra-thin c-Si solar cells

ABSTRACT

Ultra-thin crystalline silicon (c-Si) solar cells have the advantages of flexibility and light transmittance. The surface etched texture structure for reducing reflectivity usually sacrifices the flexibility of the solar cells. In this work, a kind of polydimethylsiloxane (PDMS) film with Moth-eye nanostructure was introduced to the surface of flexible ultra-thin c-Si solar cells, which was proved to enhance the flexibility of the solar cells besides reducing reflectivity and improving conversion efficiency. The finite element method was used to study the photoelectric and mechanical properties of the solar cells, the results show that the PDMS film has good flexibility to protect the ultra-thin c-Si surface, resulting in a 33.4% reduction in surface stress. At the same time, the refractive index of PDMS film with Moth-eye nanostructure has gradient change in the direction of incident light and is between that of air and c-Si. The PDMS film with Moth-eye nanostructure, as the antireflective layer on c-Si surface, reduces the reflectivity by 46.4% and improves conversion efficiency of ultra-thin c-Si solar cells by 42.3%. This work provides a method for other flexible solar cells to improve flexibility and reduce reflectivity.

## 1. Introduction

Silicon (Si) solar cells have already achieved the highest share in commercial applications due to their high conversion efficiency, mature technology and excellent stability (Luque and Hegedus, 2011). However, Si solar cells are usually about 200 μm thick, which consume a lot of Si materials, increase the cost of materials and weight, and limit application of the solar cells in portability (Han et al., 2019; Yang et al., 2016, 2018; Yoshikawa et al., 2017). The ultra-thin crystalline silicon (c-Si) solar cells reduce the thickness, effectively save the use of Si materials, and reduce the cost of materials and weight of the solar cells (Dai et al., 2019). At the same time, due to the change of thickness scale, ultra-thin c-Si solar cells have the advantages of light transmittance and flexibility (Li et al., 2016; Zhang et al., 2017). For actual demand, flexible ultra-thin c-Si solar cells can be applied to glass curtain walls, agricultural greenhouse, portable emergency chargers, etc.

The light absorption efficiency is an important factor, which determines the ability of solar cells to capture energy. According to the Yablonovitch limit, c-Si solar cells must be thick enough to achieve good light absorption (Eli and D, 1982; Green, 2002; Yablonovitch, 1982). However, the thickness of flexible ultra-thin c-Si solar cells is only tens of micrometer, and the light absorption efficiency is weak. Surface texture structures, such as pyramid, nano column, nano pore, etc., can increase incident light path and enhance the light absorption (He et al., 2017; Jeong et al., 2014, 2012; Jiang et al., 2016). These etched structures change the distribution of surface stress and destroy the flexibility of ultra-thin c-Si solar cells (Hwang et al., 2018). The flexible film with texture structure can achieve good light trapping, protect the surface and enhance the flexibility of ultra-thin c-Si solar cells. The polydimethylsiloxane (PDMS) material has good flexibility, stability, plasticity and self-cleaning (Dong et al., 2019; Dudem et al., 2016). It has suitable refractive index and low extinction coefficient, simple process and low cost, which can be used to prepare light trapping structure (Chattopadhyay et al., 2010; Choi et al., 2010; Gupta et al., 2019). PDMS films with different surface structures can be equivalent to the gradient change of refractive index in the direction of incident light according to the formula of effective medium approximation, and obtain good light trapping effect in different kinds of solar cells (Aspnes, 1982; Duan et al., 2016; Dudem et al., 2016; Khezripour et al., 2018a; Kim et al., 2019; Tavakoli et al., 2015; Xi et al., 2007; Xu et al., 2015; Zhao and Green, 1991; Khezripour et al., 2018b). Moth-eye nanostructures have been proved to be excellent light trapping

* Corresponding author.
*E-mail address:* mcli@ncepu.edu.cn (M. Li).

https://doi.org/10.1016/j.solener.2020.05.065
Received 23 January 2020; Received in revised form 14 May 2020; Accepted 21 May 2020

structures, which can be prepared on the surface of PDMS films by solution method. The surface of the Moth-eye nanostructures can be adjusted flexibly to adapt to required equivalent refractive index and its small scale can be applied to thinner films (Hashimoto and Yamamoto, 2018; Jang et al., 2017; Kang et al., 2016; Kim et al., 2019).

In this work, a kind of PDMS film with Moth-eye nanostructure is applied to the surface of ultra-thin c-Si solar cell to enhance the flexibility besides reducing reflectivity and improving conversion efficiency. The PDMS film can protect the surface of ultra-thin c-Si solar cells, and the surface stress is reduced from 53.58 to 35.85 $N{\cdot}m^{-2}$. Meanwhile, it has a good antireflective effect over the wavelength range of 300–900 nm, which increases the total light absorption of the flexible ultra-thin c-Si solar cell from 433 to 618 $W{\cdot}m^{-2}$. Finally, the conversion efficiency of the flexible ultra-thin c-Si solar cell with the PDMS film increased by 42.3%.

## 2. Simulation approach

Mechanics, optics and electricity of flexible ultra-thin c-Si solar cells are studied separately by COMSOL Multiphysics 5.4 software, which is based on the finite element method. First, mechanical calculations of ultra-thin c-Si solar cells were performed. Fig. 1(a) shows the mechanical simulation diagrammatic sketch. The thickness and length of ultra-thin c-Si are set as 10 μm and 1 mm respectively, whose left side is set as fixed constraint and right side is set as boundary load of 0.1 $N{\cdot}m^{-2}$. Texture structures are set at the position as shown in Fig. 1(a), and smooth surface, pyramid, inverted Moth-eye and Moth-eye nanostructures are simulated respectively. Their geometry parameters are shown in the Supporting Information Table S1. Then, the optical calculations of ultra-thin c-Si solar cells were carried out. Fig. 1(b) is a schematic diagram of an optical simulation, and the period of optical simulation is 1000 nm, which is composed of perfect matching layer (PML), air, PDMS film with different texture structures, 10 μm thick c-Si and silver electrode. The refractive index of air is set to 1, and that of other materials is based on the existing research data (Green, 2008; Gupta et al., 2019; Johnson and Christy, 1972). The direction of the incident light is opposite to the y-axis, and its polarization is along the x-axis. The geometrical parameters of the optical model are shown in Fig. 1(b), where d is the opening length of the Moth-eye. In the end, the electrical calculations of ultra-thin c-Si solar cells were carried out, which are based on the optical calculation results. We use a one-dimensional solar cell model with carrier generation and Shockley-Read-Hall recombination. Poisson equation and drift-diffusion equation are solved by software default solver. The thickness of ultra-thin c-Si solar cell is 10 μm, and its structure is shown in the Fig. 1(c), where the doping concentration of n-Si is $10^{16}$ $cm^{-3}$. The Gaussian distribution far away from the boundary is used in p-Si with a junction depth of 0.25 μm, where the doping concentration in surface is $10^{19}$ $cm^{-3}$. The electrical connections to the front and back surfaces are done with two Metal Contact features.

## 3. Results and discussion

The texture structure etched on ultra-thin c-Si changes the surface stress distribution, which has a great influence on the flexibility. According to the principle of elasticity, the surface stress analysis of ultra-thin c-Si wafer can be approximately equivalent to the thin plate mode. The bending process of ultra-thin c-Si can be regarded as the

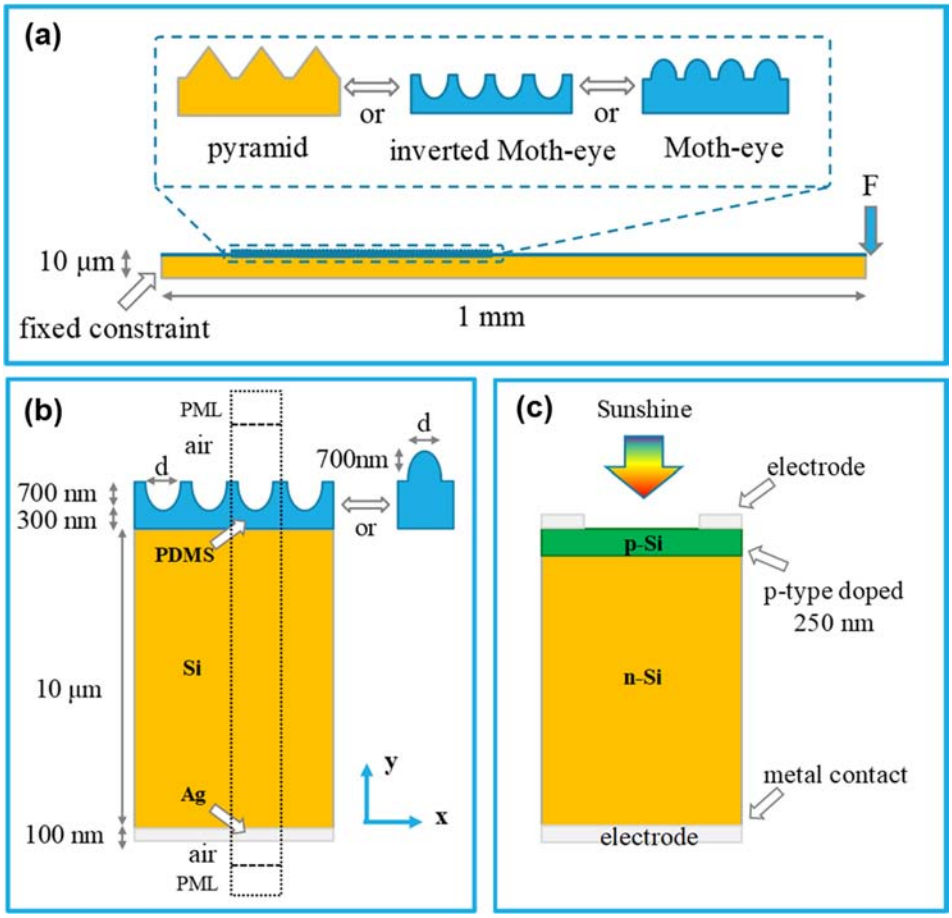


**Fig. 1.** The mechanical, optical and electrical simulation structure diagrams of ultra-thin c-Si solar cells. (a) Mechanical, (b) optical, (c) electrical simulation structure diagrams of ultra-thin c-Si solar cells.

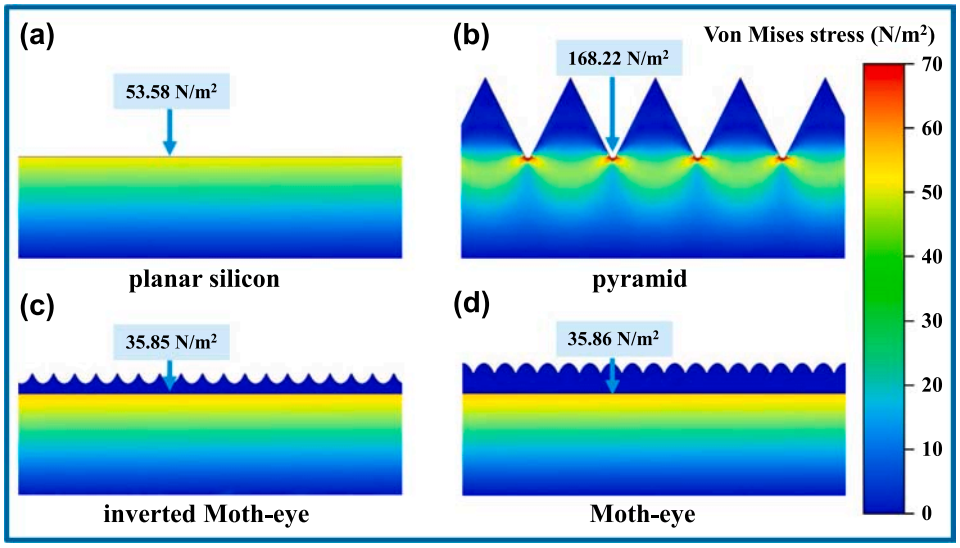


**Fig. 2.** Surface stress distributions of 10 μm thick flexible ultra-thin c-Si wafer. (a) Smooth surface, (b) pyramid, (c) inverted Moth-eye and (d) Moth-eye nanostructures PDMS films.

small deflection bending of thin plates, whose stress can be solved by Eq. (1) (Xu, 2006).

$$\left.\begin{aligned}\sigma_x &= \frac{E}{1-\upsilon^2}(\kappa_x + \upsilon\kappa_y)z\\ \sigma_y &= \frac{E}{1-\upsilon^2}(\kappa_y + \upsilon\kappa_x)z\\ \tau_{xy} &= G\kappa_{xy}z\end{aligned}\right\} \tag{1}$$

where $\sigma_x$ and $\sigma_y$ are components of normal stress, $\tau_{xy}$ is the component of shear stress, $E$ is the elastic modulus, $k_x$, $k_y$ and $k_{xy}$ are the curvature radius components of deformation, $G$ is shear modulus and $\nu$ is displacement component. From the three equations, it can be found that the stress is proportional to the elastic modulus and curvature radius, and the point of ultra-thin c-Si surface with curvature radius corresponds to larger stress. The elastic modulus is determined by the material itself. Even if the surface of PDMS film has texture structure, it has better flexibility than ultra-thin c-Si because of its small elastic modulus.

Due to the ultra-thin c-Si with a smooth surface, the curvature radius of each point on the surface is approximately equal when ultra-thin c-Si is deformed. The surface stress of the ultra-thin c-Si with smooth surface is even, which is 53.58 $N{\cdot}m^{-2}$ as shown in Fig. 2. When the ultra-thin c-Si surface with pyramid structure deforms, the deformation at the bottom of pyramids is smaller, and the deformation at the junction of pyramids is larger. This means that the curvature radius at the bottom of pyramids is small and the curvature radius at the junction of pyramids is large. The stress is mainly concentrated at the junction of pyramids, which is 168.22 $N{\cdot}m^{-2}$, three times larger than that of the ultra-thin c-Si with smooth surface, greatly reducing the flexibility of the ultra-thin c-Si wafer. Under the same deformation of the PDMS film on the ultra-thin c-Si surface, the surface stress of PDMS film is much smaller than that of ultra-thin c-Si because of its small elastic modulus. The stresses of the ultra-thin c-Si surface with the inverted Moth-eye and Moth-eye nanostructures PDMS films are 35.85 $N{\cdot}m^{-2}$ and 35.86 $N{\cdot}m^{-2}$ respectively, about 33.09% lower than that of the ultra-thin c-Si with smooth surface. Therefore, the PDMS film with texture structure also has good flexibility, which can protect the surface of the ultra-thin c-Si.

According to Fresnel formula, when light is incident from one medium to another, the greater the refractive index difference between the two mediums is, the higher the reflectivity is. The ultra-thin c-Si with smooth surface has a strong reflectivity because its refractive index is between 3.4 and 7 as shown in Fig. 3(a), which is much higher than that of air. Building a refractive index with multiple gradient changes between air and the c-Si can reduce reflectivity and increase light absorption of the c-Si (Xi et al., 2007). The red line in Fig. 3(a) is the refractive index of PDMS film, which is between that of air and the c-Si, and can be used as antireflective material on the c-Si (Gupta et al., 2019). We have studied PDMS films with inverted Moth-eye and Moth-eye nanostructures for the ultra-thin c-Si.

$$\frac{f_1(N_{PDMS}^2 - N_{eff}^2)}{(N_{PDMS}^2 + 2N_{eff}^2)} + \frac{f_2(N_{air}^2 - N_{eff}^2)}{(N_{air}^2 + 2N_{eff}^2)} = 0 \tag{2}$$

where $f_1$ and $f_2$ are the ratio of volume filling of Moth-eye nanostructure PDMS films and air, respectively, $N_{PDMS}$, $N_{air}$ and $N_{eff}$ are refractive indices of PDMS, air and equivalent layer, respectively(Duan et al., 2016). The inverted Moth-eye and Moth-eye nanostructure PDMS films can be equivalent to multiple layers with gradient refractive index by effective medium approximation Eq. (2), and the trend of that is shown in Fig. 3(b) and (d) (Khezripour et al., 2018a; Kubota et al., 2015; Noboru et al., 2011; Khezripour et al., 2018b). It is found that the variation trends of refractive index corresponding to the two structures are different, which will result in different reflectivity. There is a large step change in refractive index from PDMS to c-Si, resulting a considerable amount of reflected light from Si to PDMS. However, this reflected light does not transmit completely from the PDMS film to the air due to the gradient refractive index. It can be concluded that the reflectivity of solar cells will be greatly reduced by adding PDMS film with Moth-eye nanostructures.

According to the Yablonovitch limit, the light absorption is mainly related to the extinction coefficient and the thickness of material (Eli and D, 1982; Green, 2002; Yablonovitch, 1982). Fig. 4 shows the simulation results of reflectivity of 10 μm thick ultra-thin c-Si solar cells without rear electrode and with rear electrode. It is found that the reflectivity of light with wavelength greater than 900 nm is higher. The extinction coefficient of the c-Si is relatively low in this wavelength range. The light absorption of ultra-thin c-Si solar cells in this wavelength range is weak, and part of the reflectivity is caused by the rear electrode reflection escaping from the front surface. In order to improve the total light absorption capacity of ultra-thin c-Si solar cells, it is necessary to ensure the light absorption within the wavelength range of 300–900 nm with large extinction coefficient of c-Si. The PDMS film with nanometer Moth-eye structure has obvious antireflective effect on the wavelength range.

Compared with the reflectivity of ultra-thin c-Si solar cells without

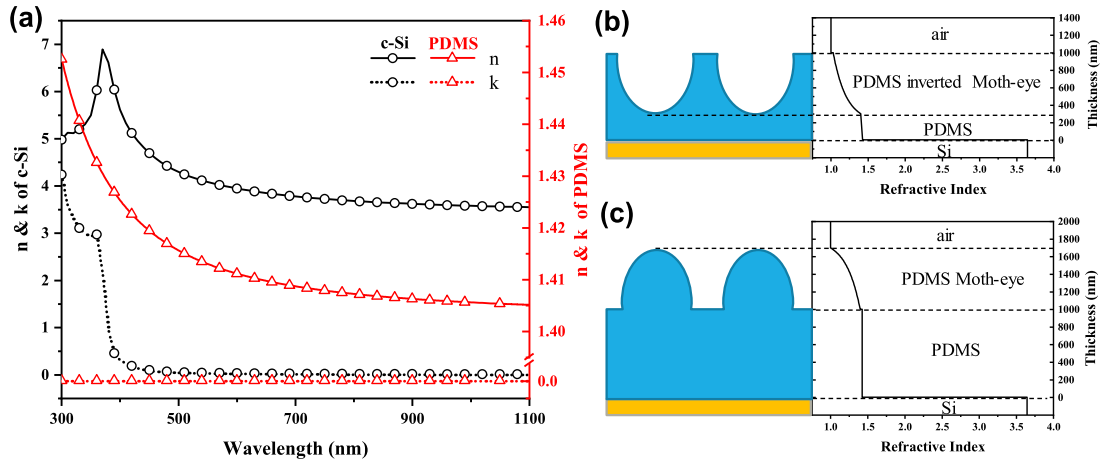


**Fig. 3.** Refractive indexes of the c-Si, PDMS, PDMS film with inverted Moth-eye and with Moth-eye nanostructures. (a) The complex refractive indexes of c-Si and PDMS film, the refractive indexes of PDMS films with (b) inverted Moth-eye and (c) Moth-eye changes in the height direction.

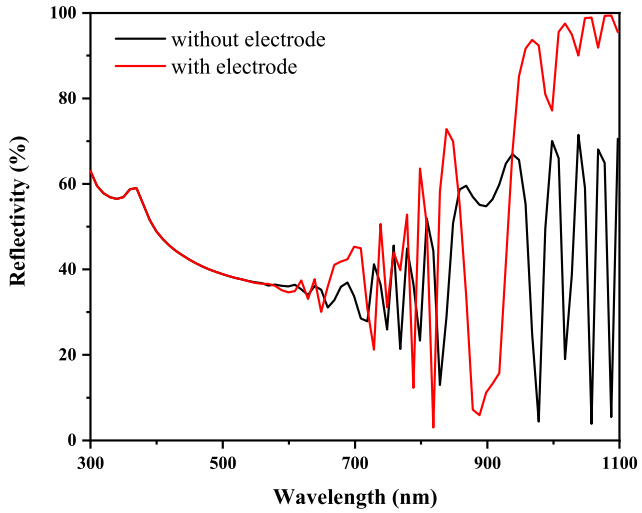


**Fig. 4.** The reflectivity of smooth surface ultra-thin c-Si solar cells without electrode and with electrode.

PDMS films, that of the solar cells with texture structure PDMS films is significantly reduced in the wavelength range of 300–900 nm. There are differences in reflectivity spectra of two different Moth-eye nanostructures in PDMS films, as shown in Fig. 5. In the inverted Moth-eye nanostructure, the main changes of reflectivity spectra are in the middle wavelength range. With d increasing, the reflectivity of the solar cells increases in the wavelength range of 300–400 nm, and decreases in the wavelength range of 400–700 nm. The total reflectivity of the solar cells with inverted Moth-eye structure PDMS film reduces by 37.4% compared with that of the reference. While the solar cells have the Moth-eye nanostructure PDMS film, the main changes of reflectivity spectra are in the short and long wavelength ranges. With the d increasing, the reflectivity of solar cells first decreased and then increased, especially at the wavelength of 970 nm. The difference of reflectivity between the two structures is due to the opening direction of Moth-eye. While the d of Moth-eye nanostructure is 800 nm, the total reflectivity is the lowest, which reduces 46.4% compared with the reference.

In order to explore the influence of geometrical parameters of two Moth-eye nanostructures on the reflectivity, we selected three special wavelengths, including 500, 900 and 970 nm, to calculate the electric field distribution. Different shapes can modulate the electric field distribution, there are different types of electric field distribution between the inverted Moth-eye and Moth-eye nanostructures. It can be discovered from the Fig. 6(a) that the Moth-eye nanostructures have a convergence effect on light, such as the effect of concave mirror. The structure of the inverted Moth-eye has a two-way converging effect, the opening has a converging effect on the electric field in the air, and the boundary of period has a converging effect on the electric field in the PDMS film. In the Moth-eye nanostructure, there is only an obvious converging effect on the electric field in the PDMS film. At the

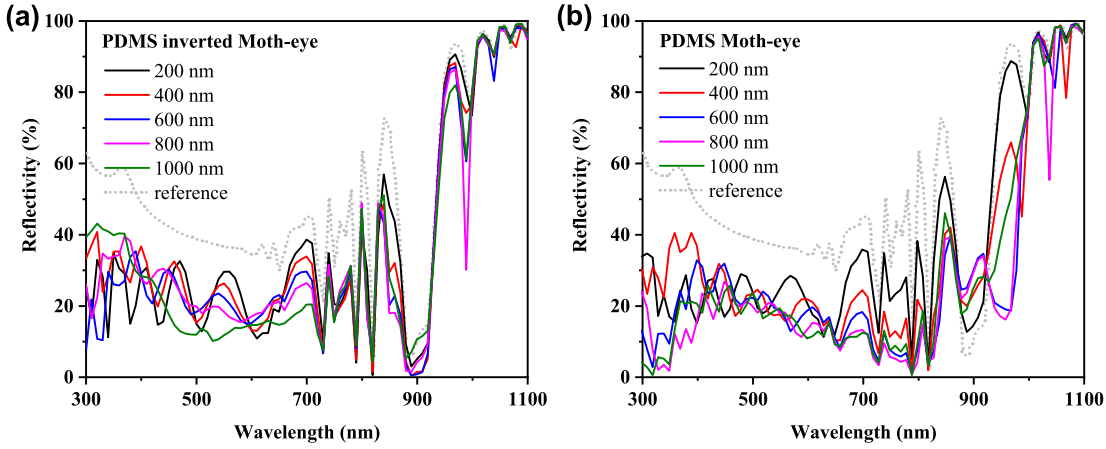


**Fig. 5.** The reflectivity of ultra-thin c-Si solar cells with inverted Moth-eye and Moth-eye nanostructures PDMS films, the reference is ultra-thin c-Si solar cells with smooth surface and rear electrode. The reflectivity of the solar cells with (a) the inverted Moth-eye and (b) Moth-eye nanostructures PDMS films with different d.

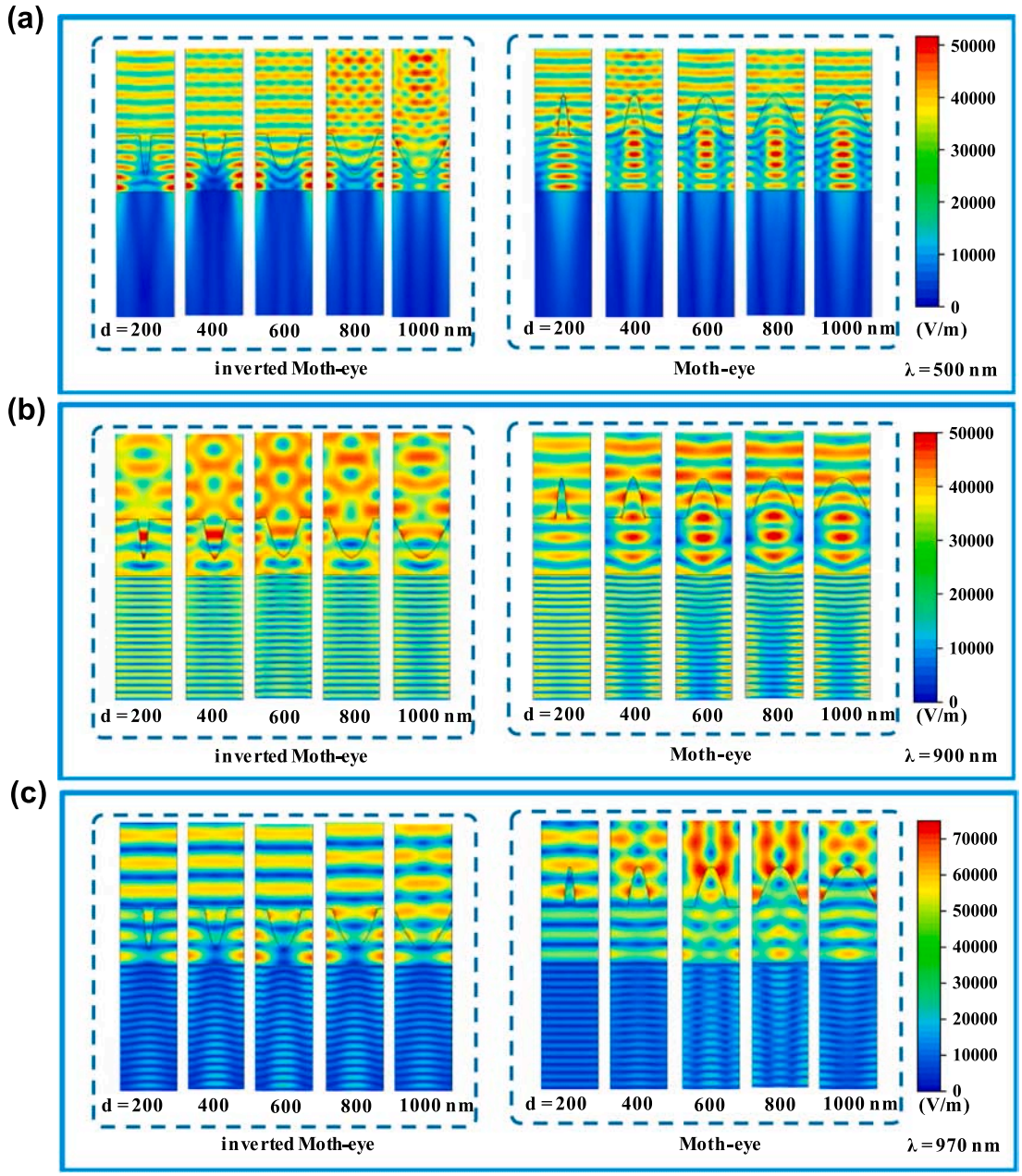


**Fig. 6.** Electric field distributions of ultra-thin c-solar cells. Electric field distributions of ultra-thin c-Si solar cells with inverted Moth-eye and Moth-eye nanostructures PDMS films at wavelength of (a) 500 nm, (b) 900 nm and 970 nm.

wavelength of 900 nm, the reflectivity of the two structures is obviously different. The reflectivity of the inverted structure is close to that of the reference, and the reflectivity of the positive structure is higher than that of the reference. From the analysis of electric field distribution, the intensity of interference fringes in c-Si with inverted Moth-eye nanostructure is lower than that in c-Si with Moth-eye nanostructure. When the wavelength is 970 nm, the reflectivity of the inverted Moth-eye nanostructure changes little, and that of the Moth-eye nanostructure first decreases and then increases with the d increasing. We can get the trend of change that is familiar with the reflectivity in Fig. 6(c). As the d increases, the intensity of interference fringes in c-Si with inverted Moth-eye nanostructure is basically same, that in c-Si with Moth-eye nanostructure first increases and then decreases. The influence of specific shape on electric field distribution should be considered in the antireflective structure.

The total light absorption of ultra-thin c-Si solar cells is an important factor determining the output current. We make statistics on the absorbed light energy density and photon flux density, and the formulas are as follows:

$$A_\tau = \int [1 - R(\lambda) - T(\lambda)] \times I(\lambda) d\lambda \tag{3}$$

$$\hat{\Gamma}_\tau = \int \frac{\lambda}{hc} [1 - R(\lambda) - T(\lambda)] \times I(\lambda) d\lambda \tag{4}$$

where $A_\tau$ is the absorbed light energy density, $R(\lambda)$ is reflectivity, $T(\lambda)$ is transmissivity, $I(\lambda)$ is spectral irradiance of AM 1.5G, $\Phi_\tau$ is the absorbed photon flux density, λ is wavelength, $h$ is the Planck constant, $c$ is the speed of light in vacuum (ASTM G-173, 2003). The statistical results are shown in Fig. 7, in which the light absorption energy density and photon flux density of ultra-thin c-Si solar cells with electrode and without texture structure PDMS film are 433 $W \cdot m^{-2}$ and $1.39 \times 10^{20}$ $m^{-2} \cdot s^{-1}$, respectively. The ultra-thin c-Si with electrodes and without texture structure were used as a reference for comparison with other light trapping structures. When the d is 1000 nm, the light absorption of

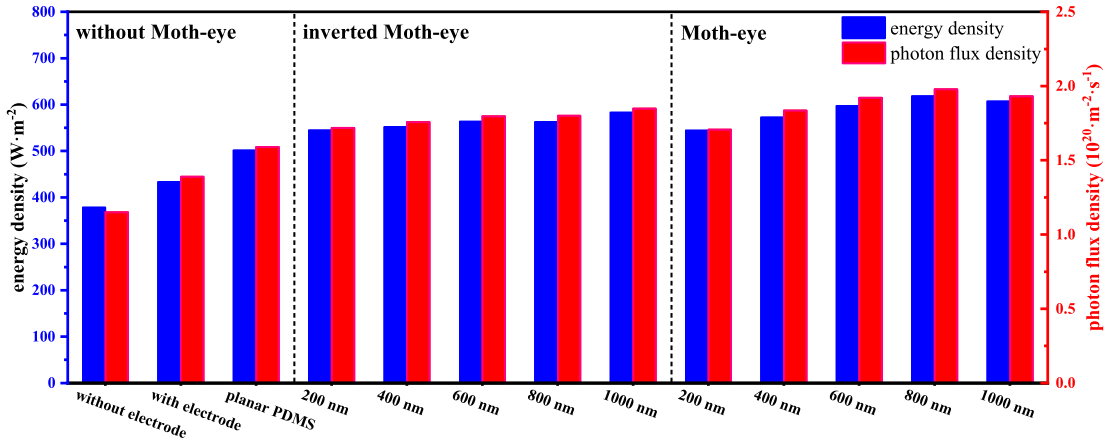


**Fig. 7.** The energy density and photon flux density absorbed by ultra-thin c-Si solar cells with different antireflective structures.

ultra-thin c-Si solar cells with inverted Moth-eye is the highest, and the energy density and photon flux density are 582 W·m$^{-2}$ and 1.85 × $10^{20}$ m$^{-2}$·s$^{-1}$ respectively, which are 1.32 times of reference. When the d is 800 nm, the light absorption of ultra-thin c-Si solar cells with Moth-eye nanostructure is the highest, and the energy density is 618 W·m$^{-2}$ and photon flux density is 1.98 × $10^{20}$ m$^{-2}$·s$^{-1}$, which are 1.42 times of reference. The light absorption of ultra-thin c-Si solar cells with Moth-eye nanostructure PDMS films was significantly improved.

The electrical simulations of ultra-thin c-Si solar cells were carried out based on the optical calculation results to study the effect of the PDMS film with Moth-eye nanostructure on the electrical performance of the solar cells. In this electrical model, the generation rate ($G$) was defined as:

$$G(z) = \int \alpha(\lambda)(1 - R(\lambda))\phi(\lambda)\exp(-i(\lambda\alpha)z)d\lambda \tag{5}$$

$$\alpha(\lambda) = \frac{4\pi\kappa(\lambda)}{\lambda} \tag{6}$$

$$\phi(\lambda) = \frac{\lambda}{\mathrm{hc}} I(\lambda) \tag{7}$$

where $z$ is the coordinate in the direction of the incident light, $\alpha(\lambda)$ is the absorption coefficient, $k(\lambda)$ is the imaginary part of the refractive index and $\Phi(\lambda)$ is the photon generation rate. Because the reflectivity includes the surface reflection and the light escaping from the front surface after the rear electrode reflection, it is approximately assumed that light entering c-Si is absorbed after several times of reflection from the front surface and rear electrode.

According to the total photon flux density absorbed by ultra-thin c-Si solar cells, the electrical performance of four solar cells has been studied, which are the solar cells without surface antireflective structure, with the planar PDMS film, with inverted Moth-eye and Moth-eye nanostructure PDMS films. The reference is the solar cells without antireflective structure, the d of the inverted Moth-eye nanostructure is 1000 nm and that of the Moth-eye nanostructure is 800 nm. It can be found that the short-circuit current density ($J_{SC}$) of ultra-thin c-Si solar cells with Moth-eye nanostructure PDMS film is obviously increased in the Fig. 8. Electric output characteristics of ultra-thin c-Si solar cells are summarized in Table 1. Ultra-thin c-Si solar cells with the Moth-eye nanostructure PDMS film display an open circuit voltage ($V_{OC}$) of 565 mV, $J_{SC}$ of 21.11 mV·cm$^{-2}$, and a fill factor of 81.83%, which yield an efficiency of 9.76%. While the solar cells with a smooth surface exhibit an efficiency of 6.86% with a $V_{OC}$ of 557 mV, a $J_{SC}$ of 15.06 mA·cm$^{-2}$, and a fill factor of 81.78%. Its efficiency is about 29.7% lower than the solar cell based on ultra-thin c-Si with Moth-eye nanostructure PDMS films, which d is 800 nm.

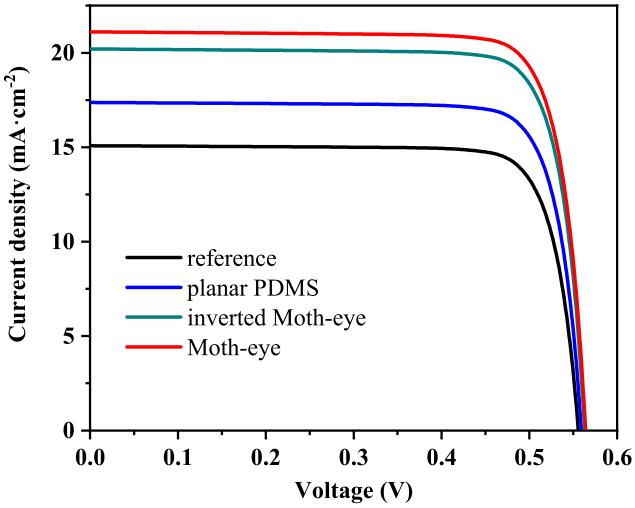


**Fig. 8.** Current density-voltage curves of ultra-thin c-Si solar cells with different surface light trapping structures, where the d of inverted Moth-eye is 1000 nm, that of Moth-eye is 800 nm.

**Table 1**
Electric output characteristics of ultra-thin c-Si solar cells with different surface light trapping structures.

| | $V_{OC}$ (mV) | $J_{SC}$ (mA·cm$^{-2}$) | Fill actor (%) | Efficiency (%) |
|---|---|---|---|---|
| Reference | 557 | 15.06 | 81.78 | 6.86 |
| Planar PDMS | 560 | 17.36 | 81.85 | 7.95 |
| Inverted Moth-eye | 564 | 20.2 | 81.83 | 9.32 |
| Moth-eye | 565 | 21.11 | 81.83 | 9.76 |

## 4. Conclusion

In summary, a kind of PDMS film with inverted Moth-eye and Moth-eye nanostructures is applied to the surface of flexible ultra-thin c-Si solar cells. We use the finite element method to study the mechanics, optics and electricity of the solar cells, and prove that PDMS films can increase the flexibility besides reducing reflectivity and improving conversion efficiency of the solar cells. PDMS films with surface texture structure can have good flexibility due to its small elastic modulus. It can protect the flexible ultra-thin c-Si solar cells and the stress on the c-Si surface is reduced by 33.4%. At the same time, the refractive index of PDMS film with texture structure is between that of air and c-Si, which can be equivalent to the refractive index with gradient change in the direction of incident light according to effective medium approximation. Compared with the total light absorption of ultra-thin c-Si solar

cells with smooth surface, that of the solar cells with inverted Moth-eye nanostructure increased by 32.9%, and that of the solar cells with Moth-eye nanostructure increased by 42.3%. The conversion efficiency of ultra-thin c-Si solar cells increased from 6.86% to 9.76%, and the $V_{OC}$ increased from 557 mV to 565 mV, when Moth-eye nanostructure PDMS films with d of 800 nm were applied. This kind of PDMS film with Moth-eye nanostructure can be used in other flexible solar cells for both antireflective and flexibility.

## Acknowledgements

This work is supported partially by National Natural Science Foundation of China (Grant nos. 51772096 and 51972110), Beijing Science and Technology Project (Z181100005118002), Par-Eu Scholars Program, Science and Technology Beijing 100 Leading Talent Training Project, the Fundamental Research Funds for the Central Universities (2017ZZD02) and the NCEPU “Double First-Class” Graduate Talent Cultivation Program.

## Appendix A. Supplementary material

Supplementary data to this article can be found online at https://doi.org/10.1016/j.solener.2020.05.065.

## References

Aspnes, D.E., 1982. Local-field effects and effective-medium theory: a microscopic perspective. Am. J. Phys. 50 (8), 704–709.
ASTM G-173, 2003. http://rredc.nrel.gov/solar/spectra/am1.5/ASTMG173/ASTMG173.html.
Chattopadhyay, S., Huang, Y.F., Jen, Y.J., Ganguly, A., Chen, K.H., Chen, L.C., 2010. Anti-reflecting and photonic nanostructures. Mat. Sci. Eng. R 69 (1–3), 1–35.
Choi, K., Park, S.H., Song, Y.M., Lee, Y.T., Hwangbo, C.K., Yang, H., Lee, H.S., 2010. Nano-tailoring the surface structure for the monolithic high-performance antireflection polymer film. Adv. Mater. 22 (33), 3713–3718.
Dai, H., Yang, L., He, S., 2019. < 50-μm thin crystalline silicon heterojunction solar cells with dopant-free carrier-selective contacts. Nano Energy 64, 103930.
Dong, W.J., Kim, S., Park, J.Y., Yu, H.K., Lee, J.-L., 2019. Ultrafast and chemically stable transfer of Au nanomembrane using a water-soluble NaCl sacrificial layer for flexible solar cells. ACS Appl. Mater. Interfaces 11(33), 30477–30483.
Duan, Z., Li, M., Mwenya, T., Fu, P., Li, Y., Song, D., 2016. Effective light absorption and its enhancement factor for silicon nanowire-based solar cell. Appl. Opt. 55 (1), 117–121.
Dudem, B., Heo, J.H., Leem, J.W., Yu, J.S., Im, S.H., 2016. CH3NH3PbI3 planar perovskite solar cells with antireflection and self-cleaning function layers. J. Mater. Chem. A 4 (20), 7573–7579.
Eli, Y., D., C.G., 1982. Intensity enhancement in textured optical sheets for solar Cells. IEEE Trans. Antennas Propag. 29(2), 300–305.
Green, M.A., 2002. Lambertian light trapping in textured solar cells and light-emitting diodes: analytical solutions. Prog. Photovoltaics 10 (4), 235–241.
Green, M.A., 2008. Self-consistent optical parameters of intrinsic silicon at 300K including temperature coefficients. Sol. Energy Mater. Sol. Cells 92 (11), 1305–1310.
Gupta, V., Probst, P.T., Gossler, F.R., Steiner, A.M., Schubert, J., Brasse, Y., Konig, T.A.F., Fery, A., 2019. Mechanotunable surface lattice resonances in the visible optical range by soft lithography templates and directed self-assembly. ACS Appl. Mater. Interfaces 11 (31), 28189–28196.
Han, C., Mazzarella, L., Zhao, Y., Yang, G., Procel, P., Tijssen, M., Montes, A., Spitaleri, L., Gulino, A., Zhang, X., Isabella, O., Zeman, M., 2019. High-mobility hydrogenated fluorine-doped indium oxide film for passivating contacts c-Si solar cells. ACS Appl. Mater. Interfaces 11 (49), 45586–45595.
Hashimoto, Y., Yamamoto, T., 2018. Fabrication of an anti-reflective and super-hydrophobic structure by vacuum ultraviolet light-assisted bonding and nanoscale pattern transfer. Micromachines 9 (4), 186.
He, Jian, Gao, Pingqi, Yang, Zhenhai, Yu, Jing, Yu, Wei, Zhang, Yu, Sheng, Jiang, Ye, Jichun, Amine, Joseph Chen, Cui, Yi, 2017. Silicon/organic hybrid solar cells with 16.2% efficiency and improved stability by formation of conformal heterojunction coating and moisture-resistant capping layer. Adv. Mater. 29 (15), 1606321.
Hwang, I., Um, H.-D., Kim, B.-S., Wober, M., Seo, K., 2018. Flexible crystalline silicon radial junction photovoltaics with vertically aligned tapered microwires. Energy Environ. Sci. 11 (3), 641–647.
Jang, S., Kang, S.M., Choi, M., 2017. Multifunctional Moth-Eye $TiO_2$/PDMS Pads with High Transmittance and UV Filtering. ACS Appl. Mater. Interfaces 9 (50), 44038–44044.
Jeong, H., Song, H., Pak, Y., Kwon, I.K., Jo, K., Lee, H., Jung, G.Y., 2014. Enhanced light absorption of silicon nanotube arrays for organic/inorganic hybrid solar cells. Adv. Mater. 26 (21), 3445–3450.
Jeong, S., Garnett, E.C., Wang, S., Yu, Z., Fan, S., Brongersma, M.L., McGehee, M.D., Cui, Y., 2012. Hybrid silicon nanocone-polymer solar cells. Nano Lett. 12 (6), 2971–2976.
Jiang, B., Li, M., Liang, Y., Bai, Y., Song, D., Li, Y., Luo, J., 2016. Etching anisotropy mechanisms lead to morphology-controlled silicon nanoporous structures by metal assisted chemical etching. Nanoscale 8 (5), 3085–3092.
Johnson, P.B., Christy, R.W., 1972. Optical constants of the noble metals. Phys. Rev. B 6 (12), 4370–4379.
Kang, S.M., Jang, S., Lee, J.-K., Yoon, J., Yoo, D.-E., Lee, J.-W., Choi, M., Park, N.-G., 2016. Moth-eye $TiO_2$ layer for improving light harvesting efficiency in perovskite solar cells. Small 12 (18), 2443–2449.
Khezripour, Z., Mahani, F.F., Mokhtari, A., 2018. Optimized design of silicon-based moth eye nanostructures for thin film solar cells. In: 2018 3rd Conference on Swarm Intelligence and Evolutionary Computation (CSIEC), pp. 1–4.
Khezripour, Z., Fouladi Mahani, F., Mokhtari, A., 2018a. Double-sided $TiO_2$ nano-gratings for broadband performance enhancement of organic solar cells. J. Opt. Soc. Am. B 35 (10).
Kim, M.-C., Jang, S., Choi, J., Kang, S.M., Choi, M., 2019. Moth-eye structured polydimethylsiloxane films for high-efficiency perovskite solar cells. Nano-Micro Lett. 11 (1).
Kubota, S., Kanomata, K., Ahmmad, B., Mizuno, J., Hirose, F., 2015. Optimized design of moth eye antireflection structure for organic photovoltaics. J. Coat. Technol. Res. 13 (1), 201–210.
Li, Y., Fu, P., Li, R., Li, M., Luo, Y., Song, D., 2016. Ultrathin flexible planar crystalline-silicon/polymer hybrid solar cell with 5.68% efficiency by effective passivation. Appl. Surf. Sci. 366, 494–498.
Luque, A., Hegedus, S., 2011. Handbook of Photovoltaic Science and Engineering. Wiley.
Noboru, Y., Oanh, N.K., Toru, T., Yusuke, N., Hideki, M., 2011. Optimization of anti-reflection moth-eye structures for use in crystalline silicon solar cells. Prog. Photovoltaics 19, 134–140.
Tavakoli, M.M., Tsui, K.-H., Zhang, Q., He, J., Yao, Y., Li, D., Fan, Z., 2015. Highly efficient flexible perovskite solar cells with antireflection and self-cleaning nanostructures. ACS Nano 9 (10), 10287–10295.
Xi, J.Q., Schubert, M.F., Kim, J.K., Schubert, E.F., Chen, M., Lin, S.-Y., Liu, W., Smart, J.A., 2007. Optical thin-film materials with low refractive index for broadband elimination of Fresnel reflection. Nat. Photonics 1 (3), 176–179.
Xu, Z., 2006. Elasticity, fourth ed. Higher Education Press, Beijing.
Xu, Z., Qiao, H., Huangfu, H., Li, X., Guo, J., Wang, H., 2015. Optical absorption of several nanostructures arrays for silicon solar cells. Opt. Commun. 356, 526–529.
Yablonovitch, E., 1982. Statistical ray optics. J. Opt. Soc. Am. 72 (7).
Yang, X., Zheng, P., Bi, Q., Weber, K., 2016. Silicon heterojunction solar cells with electron selective TiOx contact. Sol. Energy Mater. Sol. Cells 150, 32–38.
Yang, Z., Gao, P., Sheng, J., Tong, H., Quan, C., Yang, X., Chee, K.W.A., Yan, B., Zeng, Y., Ye, J., 2018. Principles of dopant-free electron-selective contacts based on tunnel oxide/low work-function metal stacks and their applications in heterojunction solar cells. Nano Energy 46, 133–140.
Yoshikawa, K., Kawasaki, H., Yoshida, W., Irie, T., Konishi, K., Nakano, K., Uto, T., Adachi, D., Kanematsu, M., Uzu, H., Yamamoto, K., 2017. Silicon heterojunction solar cell with interdigitated back contacts for a photoconversion efficiency over 26%. Nat. Energy 2 (5).
Zhang, J., Zhang, Y., Song, T., Shen, X., Yu, X., Lee, S.-T., Sun, B., Jia, B., 2017. High-performance ultrathin organic-inorganic hybrid silicon solar cells via solution-processed interface modification. ACS Appl. Mater. Interfaces 9 (26), 21723–21729.
Zhao, J., Green, M.A., 1991. Optimized antireflection coatings for high-efficiency silicon solar cells. IEEE Trans. Electron Devices 38 (8), 1925–1934.